



Numerical Investigation on Periodically Time-Varying Dynamic Characteristics of Static Eccentric Squeeze Film Damper

Z. Hai-lun^{1†,2}, C. Xi¹ and Z. Ming¹

¹ Shenyang Aerospace University, School of Aero-engine, Shenyang, Liaoning, 110136, China

² Liaoning Key Laboratory of Advanced Measurement and Test Technology for Aircraft Propulsion System, Shenyang, Liaoning, 110136, China

†Corresponding Author Email: hlzhou@sau.edu.cn

(Received January 2, 2020; accepted August 29, 2020)

ABSTRACT

To study the periodically time-varying dynamic characteristics of static eccentric squeeze film damper (SFD), two models of computational fluid dynamics were established by dynamic mesh method of transient flow field. Numerical investigation was carried out for periodically time-varying dynamic characteristics of static eccentric SFD and the results were verified by theoretical formulas. As shown by the study, due to the presence of static eccentricity, oil-film damping and stiffness present distinct periodically time-varying characteristics with precession angle and their peak values occur in different circumferential positions; excessive static eccentricity will significantly alter the distribution of oil film pressure and direction of radial force of oil film. For SFD in practice, when dynamic eccentricity is smaller, the periodically time-varying characteristics are subjected to the dual influence of oil supply hole and static eccentricity. With the augment of dynamic eccentricity, the influence from oil supply hole is reduced, and the periodically time-varying characteristics are mainly embodied as the influence of static eccentricity.

Keywords: Squeeze film damper; Static eccentricity; Damping; Stiffness.

NOMENCLATURE

c	clearance	P	oil film pressure
C	oil film damping	R	radius
e	dynamic eccentric distance	t	transient motion time
e_s	static eccentricity	X	displacements of the SFD journal
d	depth of groove	Y	displacements of the SFD journal
F_t	tangential forces	Ω	precession angular velocity
F_r	radial forces	ε	eccentricity ratio
h	oil film thickness	θ	precession angle
H	depth of groove	ρ	lubricating oil density
K	oil film stiffness	μ	dynamic viscosity
L	width of oil film		
L_g	width of groove		

1. INTRODUCTION

Squeeze film damper (SFD) has been widely applied in modern aero-engines as it proved to effectively control and isolate the vibration of rotor (San Andrés *et al.* 2019). Due to the factors like gravity of a rotor system of aero-engine, assembly error and maneuvering flight (San Andrés *et al.*

2016), the inner ring center of SFD deviates from outer and the distance between them is static eccentricity.

Sykes and Holmes (1990) made experimental studies with a rotor tester in different static eccentric conditions. The study included three static eccentric conditions and the results found that static eccentricity would cause sub-harmonic vibration of

a rotor. Zhao and Hahn (1995; 1994) studied the influence of static eccentricity on the non-linear vibration response of a rotor system with traditional and floating-ring SFD. The results indicated that excessive static eccentricity of traditional SFD caused nonlinear vibration response of the rotor system while floating-ring SFD restrained that to a certain extent. Chu and Holmes (1998) studied the influence of SFD static eccentricity on the response of a rotor system and the result indicated that larger static eccentricity made the change of critical rotation speed of the rotor system. San Andrés and Vance (1987) deduced the damping coefficients equations of open-ended SFD by the method of computational fluid dynamics, and studied the damping coefficients of open-ended SFD of off-center equilibrium position with different length-diameter ratio. Lu and Rogers (1992) carried out a study of computational fluid dynamics with viscous coefficients, unsteady inertia and convective inertia from nonlinear squeeze film force, and predicted the nonlinear multi-harmonic and unsymmetrical time waveforms of the instantaneous squeeze film force for planar motions with both in-line (initial eccentricity along the *y*-axis) and out-of-line (initial eccentricity along the *z*-axis) initial eccentricities by deducing the CFD governing equations. Bonello *et al.* (2004, 2002) conducted numerical simulation and experimental study of rotor supported on SFD with static eccentricity and the results showed that with smaller static eccentricity of damper, the calculated results are more consistent with experimental one. Adiletta and Pietra (2006) tested dynamic characteristics of SFD with static eccentric in experiments and deduced theoretical formulas. Fan and Behdinan (2017) performed numerical simulation of static eccentric SFD by compressible and incompressible fluid governing equations. And the oil film pressure distributions of static eccentric SFD were analyzed.

Diaz and San Andrés (2000) studied the influence of static eccentricity on SFD damping coefficients by rotor experiment rig. In rotation state, the results of test were necessarily influenced by the factors of rolling bearing, coupler and gearbox. Therefore, in recent years, most of dynamic parameters of static eccentric SFD had been identified in non-rotating state. San Andrés (2012) obtained different states of static eccentricity of SFD through static hydraulic system on bidirectional excitation tester, and made dynamic parameter identification, theoretical analysis and oil film pressure test based on mechanical impedance method in the states including opening and sealing on both ends (San Andrés and Seshagiri, 2013), large oil film clearance (San Andrés, 2014), large amplitude orbital motions (San Andrés and Jeung, 2015) and maneuvering flight (San Andrés *et al.* 2018; San Andrés *et al.* 2016; Jeung *et al.* 2016).

When inner and outer rings of SFD are not concentric, the procession center of the journal no longer coincides with outer ring of SFD. It results in different oil film forces in different directions, and the damping and stiffness coefficients of SFD present the periodically time-varying

characteristics. However, the studies about periodically time-varying characteristics of static eccentric SFD are rare. For that, ANSYS-CFX, computational fluid dynamics (CFD) software, was introduced to study the damping, stiffness and oil film pressure distribution in different static eccentricities when SFD journal took different procession angles. Thus, it was possible to further analyze periodically time-varying dynamic characteristics of static eccentric SFD.

To guarantee the correctness of CFD simulation, numerical simulation verification is carried out with SFD theoretical model firstly.

2. DESCRIPTION OF SFD

As shown in Fig. 1, SFD mainly consists of inlet, supply groove, housing (outer ring) and journal of elastic support (inner ring), etc. Figure 2 shows the structure parameters of SFD whose values are listed in Table 1. Besides, oil supply flow is 90mL/min, lubricating oil density $\rho=885\text{kg/m}^3$, dynamic viscosity $\mu=0.023\text{ pa}\cdot\text{s}$.

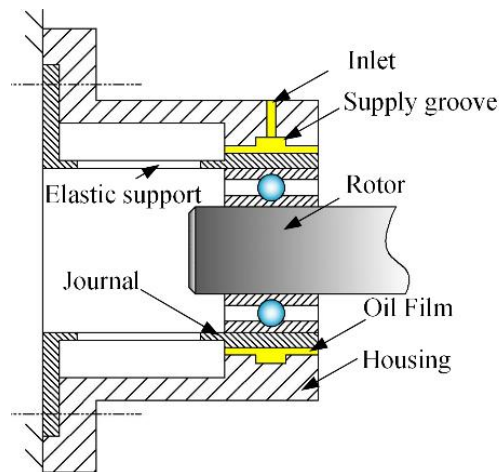


Fig. 1. Schematic diagram of SFD.

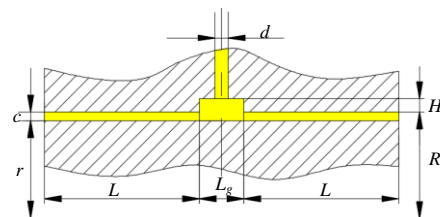


Fig. 2. SFD geometric parameters.

3. VALIDATION OF CFD SIMULATION

To verify the correctness of CFD simulation, oil film damping and stiffness formulas of concentric SFD simplified theoretical model are introduced. To facilitate the deduction of theoretical formulas, it is typical to take the left or right part of oil supply groove as the object for theoretical analysis and the simplified SFD theoretical model can be obtained as shown in Fig. 3. Based on the simplified theoretical

Table 1 Main geometric parameters of SFD (Unit: mm)

Radius	Clearance	Width of SFD	Diameter of oil supply hole	Depth of groove	Width of groove
R	c	$2L+L_g$	d	H	L_g
21.5	0.15	18	0.8	0.2	1.5

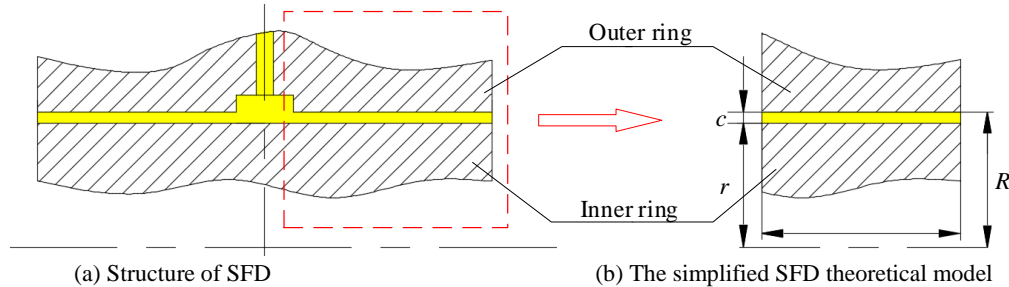


Fig. 3. SFD model.

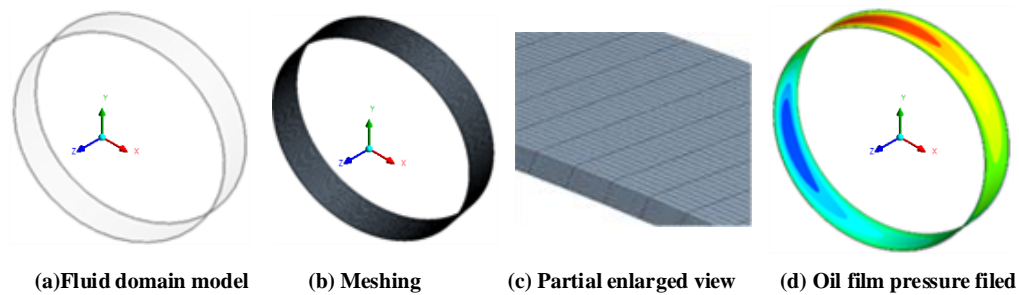


Fig. 4. CFD model and results of SFD.

model, a CFD simulation model is built by ANSYS-CFX software, as shown in Fig. 4(a). The oil film is so thin that the oil film pressure along the normal direction of journal surface is generally assumed to vary little and SFD flow state is laminar (Adiletta, 2017). The influence of mesh refinement on boundary layer is not taken into consideration during meshing. Besides, as model is in regular shape, mesh is divided by sweeping manner. The mesh is hexahedral, as shown in Fig. 4(b) and 4(c). Assume that axis orbit motion equations of the SFD journal are as follows:

$$X = e \cos(\Omega t) \quad (1)$$

$$Y = e \sin(\Omega t) \quad (2)$$

Where X and Y are the displacements of journal, e is dynamic eccentric distance, Ω is precession angular velocity, $\Omega = 503 \text{ rad/s}$ and t is transient motion time.

In the numerical simulation of ANSYS-CFX, the flow calculation field is set as dynamic mesh form. The boundary condition of inner and outer ring is “wall” that is solid (impermeable) boundary to fluid flow. The “wall” boundary condition can be set as fixed or moving as specific motion. According to the SFD motion state, SFD inner ring is set to move following Eqs. (1) and (2) and outer ring is set as

fixed. The axial ends of SFD are set as “opening” boundary (Zhu *et al.* 2002). The “opening” can be used at a boundary where the flow is into and/or out of the domain.

The number of transient calculation period is four, and the time step is 1% of one calculation cycle. The Semi-Implicit-Method for Pressure-Linked Equations is used for pressure-velocity coupling. The high-resolution solution scheme is used for overall solution accuracy. The second order backward Euler schemes is used for momentum and continuity discretization. A convergence criterion of 10^{-4} is selected for continuity and momentum residuals. After ANSYS-CFX calculation, the oil film pressure distribution can be obtained, as shown in Fig. 4(d).

In computational fluid dynamics, it is necessary to establish that the numerical solution is independent of the mesh resolution in order to verify its accuracy. The stiffness and damping are the important dynamic characteristics of SFD; therefore, they are compared for each of these meshes to determine the variation of the solution with respect to the mesh resolution (Della and Adiletta, 2002).

The tangential (F_t) and radial (F_r) forces of SFD can be obtained by integrating the pressure shown in Fig. 4(d) as follows (Zhu *et al.* 2002):

Table 2 Stiffness and damping for different mesh sizes

Mesh sizes	0.25mm	0.125mm	0.1mm
Damping (Ns/m)	106.1	122.4	123.3
Stiffness (KN/m)	17.8	12.2	12.6

Table 3 Stiffness and damping for different radial layers

Radial layers	5	10	15
Damping (Ns/m)	107.3	122.4	125.5
Stiffness (KN/m)	9.19	12.2	12.3

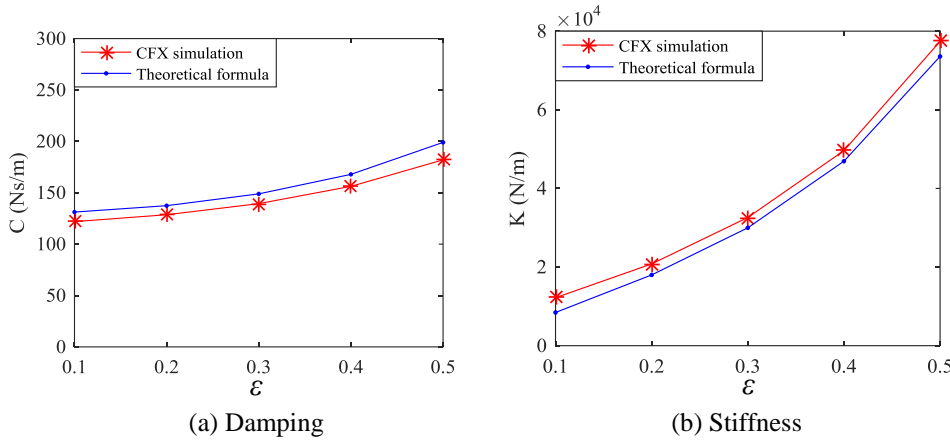


Fig. 5. Oil film damping and stiffness related with different eccentricity ratios.

$$F_r = 2 \int_0^L \int_{\theta_1}^{\theta_2} P(\theta, z) RL \sin \theta d\theta dz \quad (3)$$

$$F_t = 2 \int_0^L \int_{\theta_1}^{\theta_2} P(\theta, z) RL \cos \theta d\theta dz \quad (4)$$

Where the integrating region θ_1 and θ_2 are determined by the oil film boundary condition. The oil film limits, θ_1 and θ_2 , should take to lie at the circumferential points where P becomes zero, θ is procession angle, P is oil film pressure, R is the journal radius, L is axial length.

The damping and stiffness coefficients due to the SFD are calculated as follows (Lee *et al.* 2017; Liao, 2015):

$$C = \frac{F_t}{e\Omega} \quad (5)$$

$$K = \frac{F_r}{e} \quad (6)$$

Where C is oil film damping; K is oil film stiffness.

Let the sizes of circumference and axial meshes be equal, three different mesh sizes are selected. They are listed in the first row of Table 2. The adjusting of radial meshes size is realized by changing the layer number of radial mesh. They are listed in the first row of Table 3. The calculation results are listed in the Table 2 and Table 3 with different

mesh sizes by CFX simulation. From the Table 2 and Table 3, it can be known that the stiffness and damping tend to converge when the size of circumference and axial mesh is 0.125mm and radial layers are 10. Considering the calculation time and numerical simulation accuracy, the size of circumference and axial mesh is finalized to 0.125mm and radial layers are 10.

Based on short bearing approximation, the oil pressure P in Eqs. (3) and (4) can also be obtained by the following equation (Sarkar, 2018; Della and Adiletta, 2002):

$$P(\theta) = \frac{6\mu}{h^3} e\Omega \sin \theta (z^2 - Lz) \quad (7)$$

where z is the axial coordinate, h is oil film thickness and $h=c+e\cos\theta$. Therefore, theoretical formulas of damping and stiffness can be obtained from Eqs. (3), (4) and (7) as follows (Liao, 2015):

$$C = \frac{\mu RL^3}{c^3} \left[\frac{\pi}{2(1-\varepsilon^2)^{3/2}} \right] \quad (8)$$

$$K = \frac{\mu \Omega RL^3}{c^3} \left[\frac{2\varepsilon}{(1-\varepsilon^2)^2} \right] \quad (9)$$

Where ε is the dimensionless eccentricity ratio, $\varepsilon = e/c$.

To validate the correctness and rationality of CFX simulation, results of the CFX simulation and theoretical formula are presented in Fig. 5. It can be known that the results of the CFX simulation and theoretical formula have a good consistency in the fact that oil film damping and stiffness increases with eccentricity ratio. But there is also difference in both. The difference between them is mainly caused by short bearing approximation, neglecting the radial variation of oil film pressure and oil film inertia in the theoretical formulas.

Figure 4(d) shows that the maximum and minimum of the pressure are at top and left side. To further validate the numerical simulation, when eccentricity ratio of SFD is 0.3, the oil pressures of SFD at the middle land in Fig. 4(d) are extracted, as shown in Fig. 6. The oil pressures of SFD at the middle land can also be obtained by Eq. (7), as shown in Fig. 6. The curve with asterisks denotes CFX simulation solution, and the curve with dots denotes the theoretical formula solution. Figure 6 shows that good consistency is achieved between theoretical formula and CFX simulation result. The difference between them is mainly caused by short bearing approximation and neglecting oil film inertia in the theoretical formula.

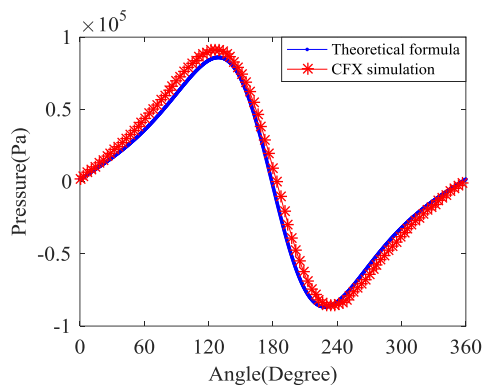


Fig 6. Oil film pressure curve at the middle land.

4 PERIODICALLY TIME-VARYING DYNAMIC CHARACTERISTICS OF STATIC ECCENTRIC SFD

4.1 Simplified Theoretical Model

Based on ANSYS-CFX model of concentric SFD, the CFX simulation of static eccentric SFD can be realized by altering the control equation of SFD journal motion orbit. By adding static eccentricity e_s to Eq. (1), the X-direction component of static eccentric SFD journal motion orbit can be obtained as follow:

$$X = e \cos(\Omega t) - e_s \quad (10)$$

The Y-direction component remains intact, so that the axis orbit motion equations of static eccentric SFD are achieved. The CFX model of static eccentric SFD can be named as model I, which is built based on simplified theoretical model of SFD.

To analyze the influence of static eccentricity on oil

film pressure of SFD, 4 monitoring points were set at axial midpoint $L/2$ and evenly distributed at circumferential 90° , as shown in Fig. 7.

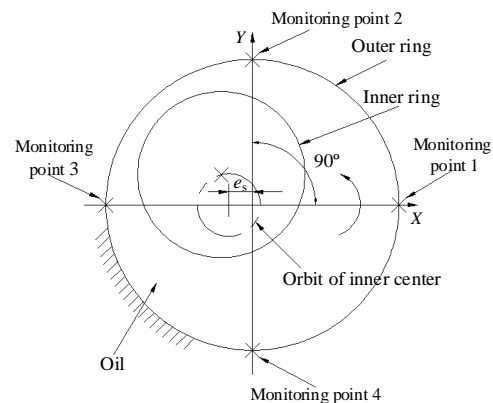


Fig. 7. Monitoring points distribution and orbit of SFD inner center.

When static eccentricity is equal to 0, oil film damping and stiffness of SFD with different dynamic eccentricities can be obtained by ANSYS-CFX simulation, as shown in Fig.8. It can be seen from the figure that when SFD journal moves to different circumferential positions, the oil film damping and stiffness is equal everywhere.

When static eccentricity is not equal to 0 and $e=0.015\text{mm}$, the oil film damping and stiffness of SFD can be obtained by ANSYS-CFX simulation under different static eccentricities, as shown in Fig. 9. It can be seen from the figure that due to the presence of static eccentricity, damping and stiffness varies greatly with different procession angles of SFD inner ring. Compared with concentric SFD shown in Fig.8, there is a great fluctuation of oil film damping and stiffness in Fig. 9. It can be seen from Fig.7 and Fig.9 that when SFD inner ring anticlockwise moves from monitoring point 1 (procession angle is 0°) to 3 (procession angle 180°), damping and stiffness increases as static eccentricity increases; damping peaks appear between monitoring point 1 (procession angle is 0°) and 3 (procession angle 180°), while stiffness peaks occur near point 3(procession angle 180°). Thus, it can be shown that peaks of damping and stiffness occur in different circumferential positions. When SFD inner ring moves from monitoring point 3 (procession angle is 180°) to 1 (procession angle 360°), variation of damping is relatively small while stiffness decreases sharply.

It can be seen from Fig. 9 (b) that when SFD inner ring moves to the position nearby 0° , there is negative stiffness. To study the cause for negative stiffness of static eccentric SFD, the circumferential distributions of oil film pressure are obtained by ANSYS-CFX simulation and diagrammatic drawings of pressure distributions are shown in

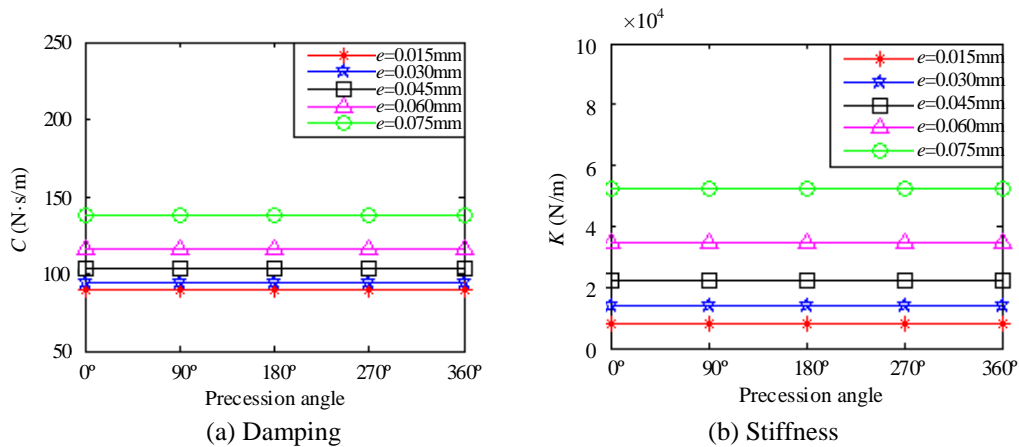


Fig. 8. Oil film damping and stiffness of concentric SFD in different circumferential positions.

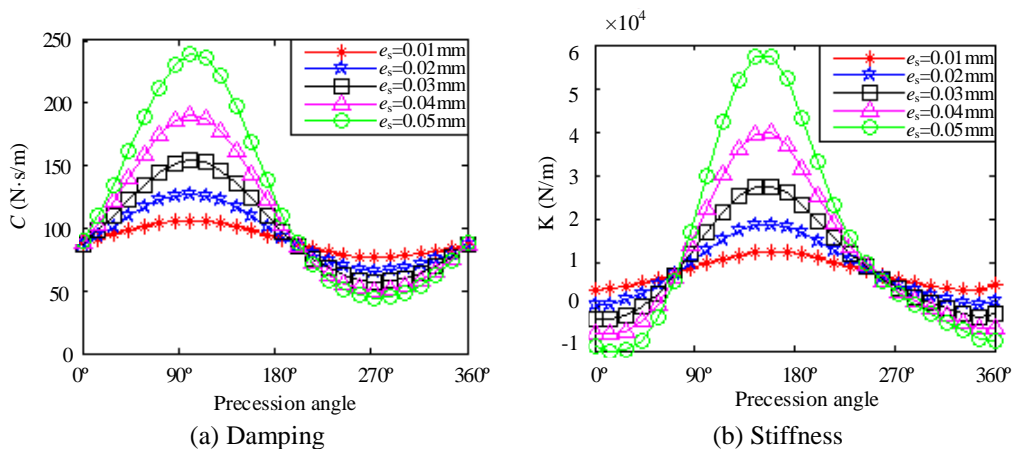


Fig. 9. Oil film damping and stiffness of SFD model I in different circumferential positions ($e=0.015\text{mm}$).

Fig.10. From Fig. 10 (a) that when SFD inner ring is at 0° position and $e_s=0$, the oil film pressure on journal is mainly distributed circumferentially in the first quartile and the oil film radial force F_r points to motion center of SFD inner ring from outside and the oil film stiffness is positive at this time; when static eccentricity e_s varies from 0.01mm to 0.05mm, the oil film pressure of journal are shown in Fig. 10 (b), (c) and (d). It can be seen from figures that the oil film pressure imposed circumferentially on journal gradually transits from the first quadrant to second. And the oil film radial force of journal F_r points to outside from motion center of journal, namely oil film stiffness gradually changes to negative value. The direction of tangential force of oil film F_t remains unchanged. Therefore, oil film damping is positive.

4.2 Actual Structure Models of Static Eccentric SFD

Simplified SFD theoretical model cannot reflect the influences from oil supply conditions. To thoroughly analyze the periodically time-varying dynamic characteristics of static eccentric SFD, a further study on the actual structure of SFD is

required.

An SFD model with oil supply can be built based on the structural sizes of SFD in Table 1. It can be named as model II. Similar to model I of SFD, the model II also can be realized. The main difference is that oil supply hole is modeled as “inlet” in model II. The oil supply flow can be set by inlet boundary. The fluid domain model, meshing and oil film pressure filed of model II are shown in Fig. 11.

When static eccentricity is not present, namely $e_s=0$, the oil film damping and stiffness can be obtained in different circumferential positions based on model II, as shown in Fig.12. Different from the results achieved by model I (as shown in Fig.8) and due to the existence of oil supply hole, oil film damping and stiffness of concentric SFD conforms to the rule of harmonic curve with different precession angles. When SFD journal anticlockwise moves from monitoring point 1 (precession angle = 0°) to 3 (precession angle = 180°), damping values are small as the oil supply pressure at oil supply hole is opposite to the tangential force of oil film (the damping force of SFD) on journal; when

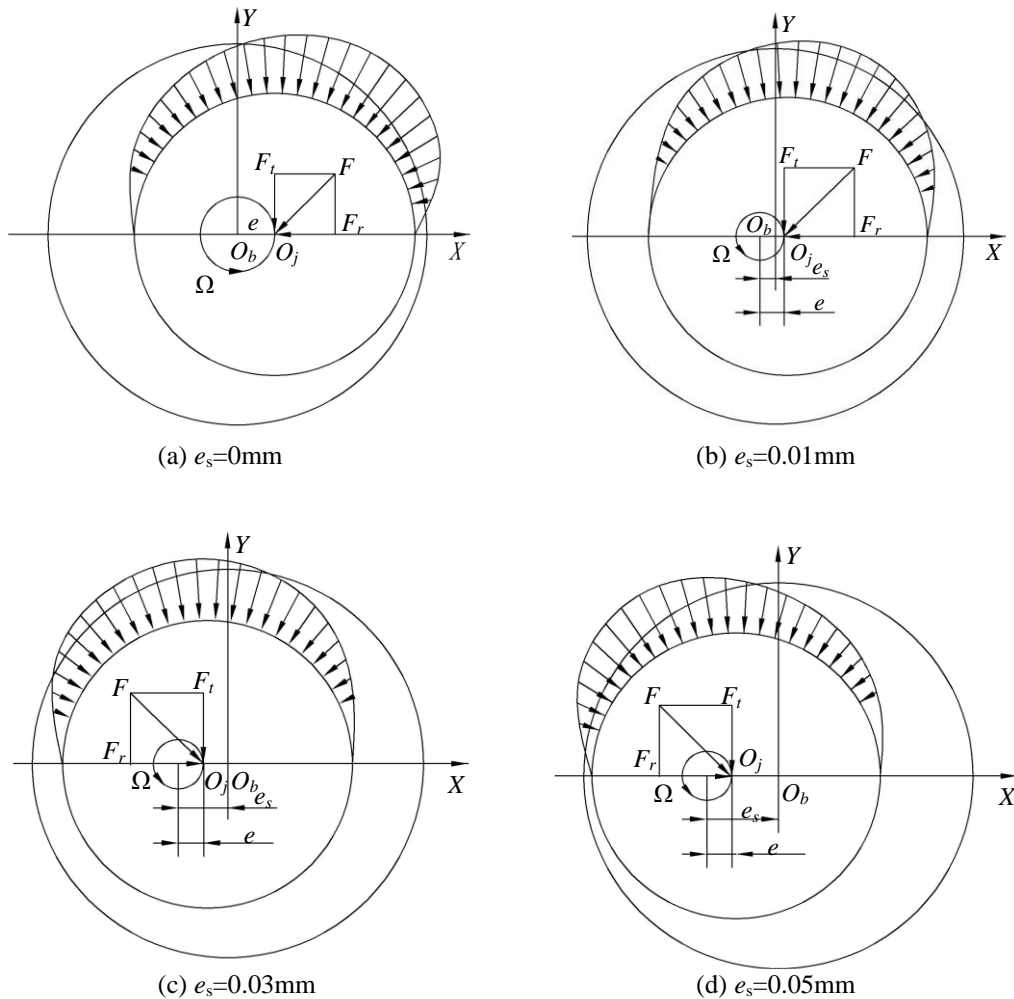


Fig. 10. Oil film pressure distributions diagrammatic drawings of SFD with different static eccentric.

moving from 3 (procession angle = 180°) to 1 (procession angle = 360°), damping values increase as oil supply pressure is the same with tangential force of oil film in direction; when moving to the positions nearby 3 (procession angle = 180°), radial force of oil film is opposite to oil supply pressure in position, and thereby the stiffness is minimum.

Let dynamic eccentricity $e=0.015\text{mm}$ and the damping and stiffness of SFD with different static eccentricities can be obtained at different procession angles through ANSYS-CFX simulation, as shown in Fig. 13. It can be seen from the figure that existence of static eccentricity significantly changes the rule of oil film damping and stiffness varying with procession angle. Due to the dual influence of oil supply and static eccentricity, the stiffness decreases first and then increases, and again in a cycle; when static eccentricity is 0.01 and 0.02mm, SFD journal moves from monitoring point 3 (procession angle = 180°) to monitoring point 1 (procession angle = 360°), damping tends to rise with procession angle increases. It can be known from Fig.12 that it is caused by oil supply hole.

In the case of larger dynamic eccentricity, oil film damping and stiffness of SFD with different static eccentricities are obtained by ANSYS-CFX simulation, as shown in Fig. 14 and Fig.15. It can be seen from the figures that with the increase of dynamic eccentricity, the peak of damping and stiffness increases significantly; the influence of oil supply hole decreases significantly with the increase of dynamic eccentricity; the variation rule of damping and stiffness is basically consistent with the result obtained by model I of static eccentric SFD.

5. CONCLUSIONS

To study periodically time-varying dynamic characteristics of static eccentric SFD, the correctness and reasonability of numerical simulation had been validated by theoretical formula of SFD with short-bearing approximation, and then ANSYS-CFX numerical simulation was carried out based on two models of static eccentric SFD. The results are shown as follow:

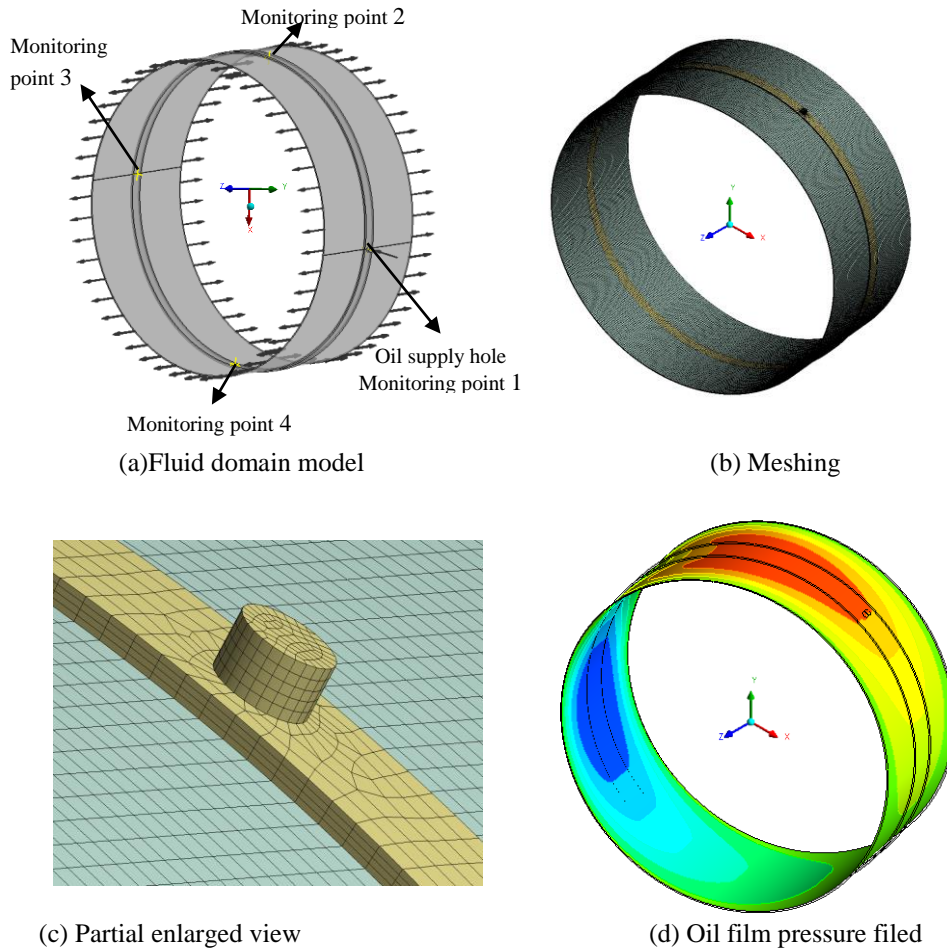


Fig. 11. Actual structural model of static eccentric SFD.

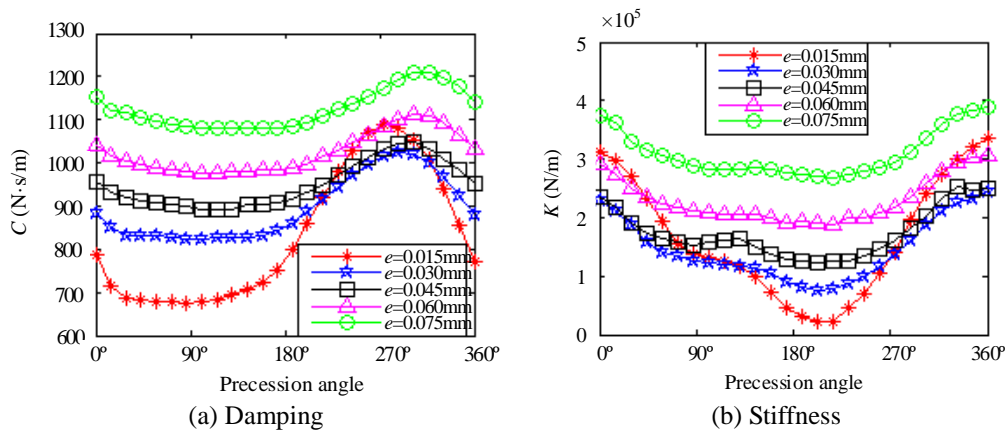


Fig. 12. Oil film damping and stiffness of concentric SFD with oil supply in different circumferential positions.

- 1) Existence of static eccentricity makes oil film damping and stiffness show periodically time-varying characteristic when SFD moves to different circumferential positions and the peak of damping and stiffness occurs in different circumferential positions in a cycle.
- 2) Excessive static eccentricity will significantly alter the distribution of oil film pressure and result in the change of radial force direction of oil film. Negative stiffness is detected in certain precession angles, but the oil film damping remains positive.

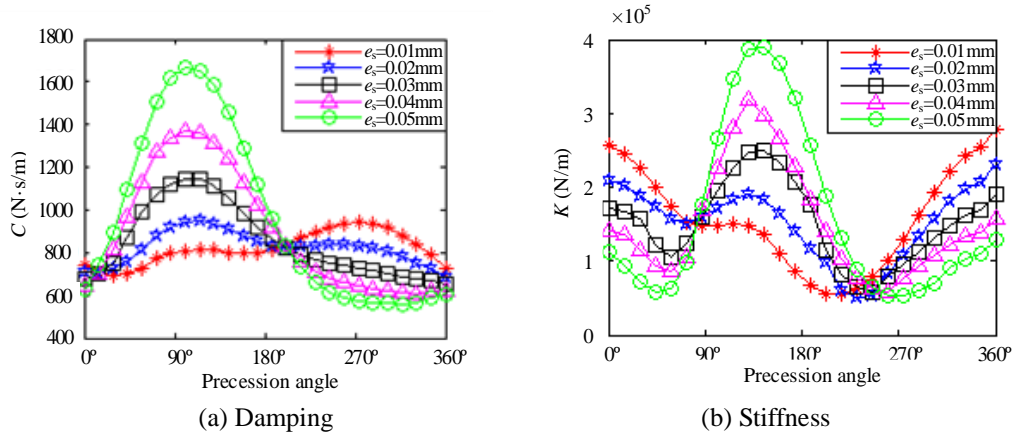


Fig. 13. Oil film damping and stiffness of SFD model II in different circumferential positions ($e=0.015\text{mm}$).

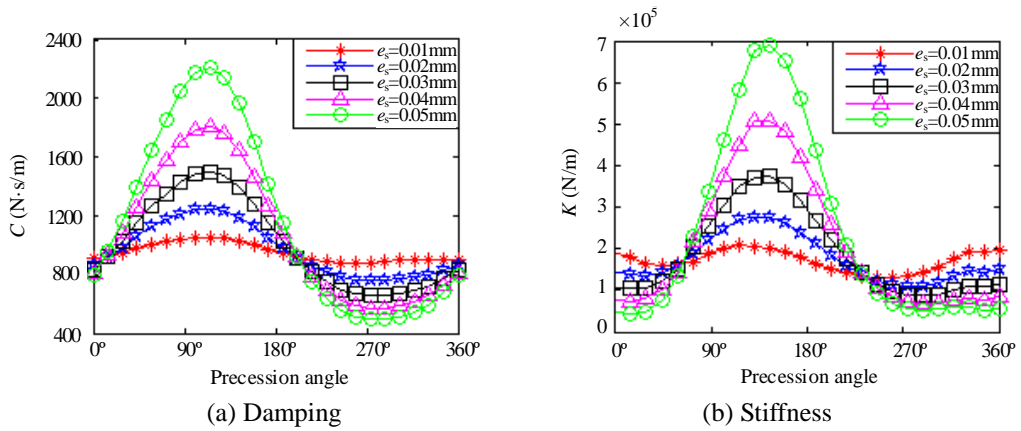


Fig. 14. Oil film damping and stiffness of SFD model II in different circumferential positions ($e=0.045\text{mm}$).

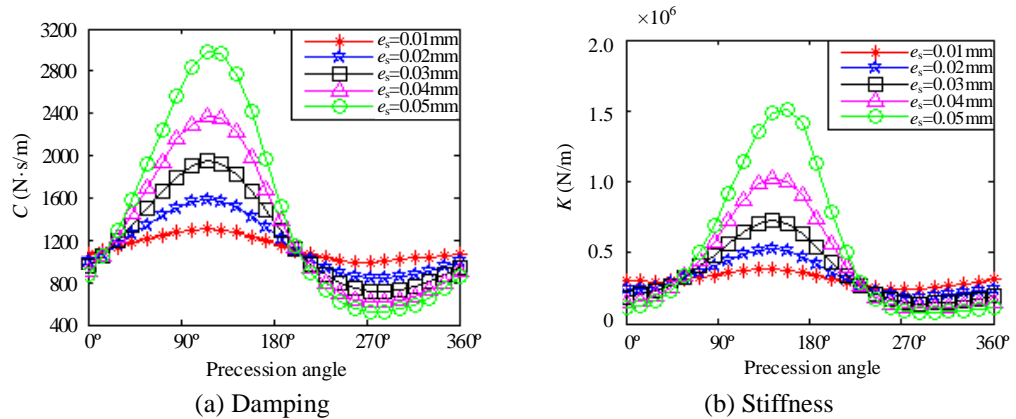


Fig. 15. Oil film damping and stiffness of SFD model II in different circumferential positions ($e=0.075\text{mm}$).

- 3) For an actual SFD without static eccentricity, due to the influence of oil supply hole, the variation of oil film damping and stiffness forms a harmonic curve with different precession angle.
- 4) Under the dual influence of oil supply and static

eccentricity, the stiffness decreases first and then increases, and again in a cycle. As the increase of dynamic eccentricity, the peak of oil film damping and stiffness increases significantly, and the influence of oil supply hole decreases significantly, and variation rule of damping and stiffness is consistent with the result obtained by simplified theoretical model

in general.

ACKNOWLEDGEMENTS

This work is financially supported by the National Natural Science Foundation of China (No. 51505300), Scientific Research Fund of Education, Science and Technology Department of Liaoning Province (No. 2019-ZD-0233, No. JYT19061).

REFERENCES

- Adiletta, G. (2017). An insight into the dynamics of a rigid rotor on two-lobe wave squeeze film damper. *Tribology International* 116, 69-83.
- Adiletta, G., and L. D. Pietra (2006). Experimental Study of a Squeeze Film Damper With Eccentric Circular Orbits. *Journal of Tribology* 128(2), 365-377.
- Bonello, P., M. J. Brennan and R. Holmes (2002). Non-linear modelling of rotor dynamic systems with squeeze film dampers—an efficient integrated approach. *Journal of Sound and Vibration* 249(4), 743-773.
- Bonello, P., M. J. Brennan and R. Holmes (2004). A Study of the Nonlinear Interaction Between an Eccentric Squeeze Film Damper and an Unbalanced Flexible Rotor. *Journal of Engineering for Gas Turbines & Power* 126(4), 855-866.
- Chu, F. and R. Holmes (1998). The Effect of Squeeze Film Damper Parameters on the Unbalance Response and Stability of a Flexible Rotor. *Journal of Engineering for Gas Turbines & Power* 120(1), 140-148.
- Della Pietra, L. and G. Adiletta (2002). The squeeze film damper over four decades of investigations. Part I: Characteristics and operating features. *The Shock and Vibration Digest* 34(1), 3-26.
- Diaz, S. and L. San Andrés (2000). Orbit-Based Identification of Damping Coefficients for a Rotor Mounted on Off-Centered Squeeze Film Dampers and Including Support Flexibility; *proceedings of the ASME Turbo Expo 2000: Power for Land, Sea, and Air*, Munich, Germany.
- Fan, T. and K. Behdinan (2017). The Evaluation of Linear Complementarity Problem Method in Modeling the Fluid Cavitation for Squeeze Film Damper with Off-Centered Whirling Motion. *Lubricants* 5(4), 1-13.
- Jeung, S. H., L. San Andrés and G. Bradley (2016). Forced Coefficients for a Short Length, Open Ends Squeeze Film Damper With End Grooves: Experiments and Predictions. *Journal of Engineering for Gas Turbines and Power* 138(2), 1-11.
- Lee, G. J., J. Kim and T. Steen (2017). Application of computational fluid dynamics simulation to squeeze film damper analysis. *Journal of Engineering for Gas Turbines and Power* 139(10), 1-11.
- Liao, M. F. (2015). *Rotor dynamics of aero-engine*. Northwestern Polytechnical University Press.
- Lu, Y. and R. J. Rogers (1992). A nonlinear model for short length cylindrical squeeze film with large planer motions, *Journal of Tribology*, 114(1), 192-198.
- San Andrés, L., M. J. Vance (1987). Force Coefficients for Open-Ended Squeeze Film Dampers Executing Small-Amplitude Motion about an Off-Center Equilibrium Position. *ASLE Transactions* 30, 69-76.
- San Andrés, L. (2012). Damping and inertia coefficients for two open ends squeeze film dampers with a central groove: measurements and predictions. *Journal of Engineering for Gas Turbines and Power* 134(10), 1-9.
- San Andrés, L. (2014). Force coefficients for a large clearance open ends squeeze film damper with a central feed groove: Experiments and predictions. *Tribology International* 71, 17-25.
- San Andrés, L. and S. Seshagiri (2013). Damping and inertia coefficients for two end sealed squeeze film dampers with a central groove: measurements and predictions. *Journal of Engineering for Gas Turbines and Power* 135(11), 1-9.
- San Andrés, L. and S. H. Jeung (2015). Experimental performance of an open ends, centrally grooved, squeeze film damper operating with large amplitude orbital motions. *Journal of Engineering for Gas Turbines and Power* 137(3), 1-9.
- San Andrés, L., B. Koo and S. H. Jeung (2019). Experimental Force Coefficients for Two Sealed Ends Squeeze Film Dampers (Piston Rings and O-Rings): An Assessment of Their Similarities and Differences. *Journal of Engineering for Gas Turbines and Power* 141, 1-13.
- San Andrés, L., S. Den and S. H. Jeung (2018). On the Force Coefficients of a Flooded, Open Ends Short Length Squeeze Film Damper: From Theory to Practice (and Back). *Journal of Engineering for Gas Turbines and Power* 140(1), 1-11.
- San Andrés, L., S. Den and S-H. Jeung (2016). Transient Response of a Short-Length ($L/D=0.2$) Open-Ends Elastically Supported Squeeze Film Damper: Centered and Largely Off-Centered Whirl Motions. *Journal of Engineering for Gas Turbines and Power* 138(12), 1-11.
- Sarkar, S. (2018). *Numerical investigation of vapor and gaseous cavitation in squeeze-film damper bearings*. MSc thesis, University of Cincinnati, Cincinnati, USA.

- Sykes, J. E. H. and R. Holmes (1990). The effect of bearing misalignment on the non-linear vibration of aero-engine rotor-damper assemblies. *Proceedings of the Institution of Mechanical Engineers Part G Journal of Aerospace Engineering* 204(27), 83-99.
- Zhao, J. Y. and E. J. Hahn (1995). Eccentric Operation and Blade-Loss Simulation of a Rigid Rotor Supported by an Improved Squeeze Film Damper. *Journal of Tribology* 117(3), 490-497.
- Zhao, J. Y., I. W. Linnett and L. J. Mclean (1994). Subharmonic and quasi-periodic motions of an eccentric squeeze film damper-mounted rigid rotor. *Journal of Vibration & Acoustics* 116(3), 357-363.
- Zhu, C., D. Robb and D. Ewins (2002). Analysis of the multiple-solution response of a flexible rotor supported on non-linear squeeze film dampers *Journal of sound and vibration* 252(3), 389-408.